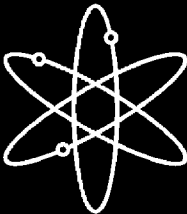
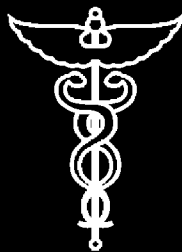


Crack Growth Rates of Nickel Alloy Welds in a PWR Environment



Argonne National Laboratory



**U.S. Nuclear Regulatory Commission
Office of Nuclear Regulatory Research
Washington, DC 20555-0001**



Crack Growth Rates of Nickel Alloy Welds in a PWR Environment

Manuscript Completed: January 2004
Date Published: May 2006

Prepared by
B. Alexandreanu, O. K. Chopra, and W. J. Shack

Argonne National Laboratory
9700 South Cass Avenue
Argonne, IL 60439

W. H. Cullen, Jr., NRC Project Manager

Prepared for
Division of Fuel, Engineering and Radiological Research
Office of Nuclear Regulatory Research
U.S. Nuclear Regulatory Commission
Washington, DC 20555-0001
NRC Job Code Y6388



Intentionally Left Blank

Crack Growth Rates of Nickel Alloy Welds in a PWR Environment

by

B. Alexandreanu, O. K. Chopra, and W. J. Shack

Abstract

In light water reactors (LWRs), vessel internal components made of nickel–base alloys are susceptible to environmentally assisted cracking. A better understanding of the causes and mechanisms of this cracking may permit less conservative estimates of damage accumulation and requirements on inspection intervals. A program is being conducted at Argonne National Laboratory to evaluate the resistance of Ni alloys and their welds to environmentally assisted cracking in simulated LWR coolant environments. This report presents crack growth rate (CGR) results for Alloy 182 shielded–metal–arc weld metal in a simulated pressurized water reactor (PWR) environment at 320°C. Crack growth tests were conducted on 1–T compact tension specimens with different weld orientations from both double-J and deep-groove welds. The results indicate little or no environmental enhancement of fatigue CGRs of Alloy 182 weld metal in the PWR environment. The CGRs of Alloy 182 in the PWR environment are a factor of ≈ 5 higher than those of Alloy 600 in air under the same loading conditions. The stress corrosion cracking for the Alloy 182 weld is close to the average behavior of Alloy 600 in the PWR environment. The weld orientation was found to have a profound effect on the magnitude of crack growth: cracking was found to propagate faster along the dendrites than across them. The existing CGR data for Ni–alloy weld metals have been compiled and evaluated to establish the effects of key material, loading, and environmental parameters on CGRs in PWR environments. The results from the present study are compared with the existing CGR data for Ni–alloy welds to determine the relative susceptibility of the specific Ni–alloy weld to environmentally enhanced cracking.

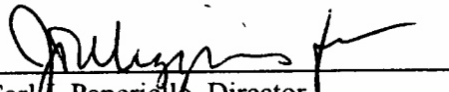
Intentionally Left Blank

Foreword

This report presents crack growth rate data and the results of the corresponding fracture surface and metallographic examinations from cyclic loading and primary water stress-corrosion cracking (PWSCC) tests of two nickel-base Alloy 182 (A182) weldments, which are typical of those used in vessel penetrations and piping butt welds in nuclear power plants. The effect of crack orientation with respect to dendrite orientation is the most significant variable investigated in this study. However, this report also includes a review of data from several laboratories, which describes the effects of material composition, loading characteristics, and chemistry of the aqueous environment. The main conclusion is that the PWSCC growth rates described for A182 specimens in this report are comparable to the crack growth rates that characterize the performance of Alloy 600 (A600).

This report is the first in a series documenting the results of crack growth rate testing in vessel head penetration materials, focusing on the weld metals, A182 and A152, and including results of some tests of the base metals, A600 and (eventually) A690. The results presented in this report were obtained in tests of a laboratory-fabricated, shielded metal arc welding deposit of A182. Testing of A182 weldments continues at Argonne National Laboratory, and substantially more crack growth rate results are anticipated in the next two years.

The impetus for this research on PWSCC comes from User Need Request NRR-2002-018, submitted by the U.S. Nuclear Regulatory Commission, Office of Nuclear Reactor Regulation. This topic may be an especially important consideration in the review of license applications, as well as the disposition of relief requests pertaining to flaw evaluations for vessel penetration and piping butt welds. The data on cyclic loading effects are commonly used in the fatigue analyses that are required for flaw evaluations completed in accordance with the requirements set forth in Section XI, IWB-3660 and Appendix O, of the Boiler and Pressure Vessel Code promulgated by the American Society of Mechanical Engineers.



Carl U. Paperiello, Director
Office of Nuclear Regulatory Research
U.S. Nuclear Regulatory Commission

Intentionally Left Blank

Contents

Abstract.....	iii
Foreword	v
Executive Summary.....	xv
Acknowledgments	xvii
Abbreviations	xix
1. Introduction	1
2. Experimental.....	3
2.1 Material and Specimen Design	3
2.2 Test Facility	5
2.3 Test Procedure.....	7
3. Microstructural Characterization.....	11
3.1 Weld Microstructure	11
3.2 Examination of Weld by SEM/EDX.....	15
3.3 Examination of Weld Specimens by Orientation Imaging Microscopy	18
4. ANL Test Results	27
4.1 Crack Growth Data	27
4.1.1 Crack Growth Data for Double-J Weld Specimen CT31-W01 TS	27
4.1.2 Crack Growth Data for Double-J Weld Specimen CT31-W02 TS	34
4.1.3 Crack Growth Data for Deep-Groove Weld Specimen CT933-TS	37
4.1.4 Crack Growth Data for Deep-Groove Weld Specimen CT933-TL.....	42
4.1.5 Crack Growth Data for Deep-Groove Weld Specimen CT933-LS	48
4.2 Effect of Grain Boundary Type and Relative Grain Orientation on Crack Propagation.....	51
5. Discussion	59
5.1 Cyclic Crack Growth Rates	59
5.1.1 Air Environment	59
5.1.2 PWR Environment.....	59

5.2. Crack Growth Rates under Constant Load	61
5.3. Effect of Key Parameters on SCC Crack Growth Rates.....	63
5.3.1 Effect of Orientation of Dendrites	63
5.3.2 Effect of Size of the Experimental Crack Advance.....	64
5.3.3 Effect of Gentle Cycling and Periodic Unloading.....	66
5.3.4 Effect of Water Chemistry	67
5.3.5 Effect of Temperature.....	68
5.3.6 Heat-to-Heat Comparisons of the CGR Data	69
5.3.7 Extrapolation of Available Data to the Population of Alloy 182 and 82 Weld Materials.....	70
6 Summary.....	75
References	77

Figures

1.	Configuration of compact-tension specimen used for this study.	3
2.	Schematic of the weld joint design and weld passes.	4
3.	Orientation of the CT specimen from the Alloy 182 SMA weld.	4
4.	A photograph of the facility for conducting crack growth tests in simulated LWR environments.	5
5.	A photograph of the specimen load train.	6
6.	Schematic diagram of the recirculating autoclave system used for crack growth rate tests.	6
7.	Schematic showing the locations of the three samples cut from the weld.	11
8.	Weld microstructure from Sample 1; transition area between the weld and Alloy 600; and dendritic microstructure in the weld.	12
9.	Large grain microstructure in the HAZ at two opposite positions.	13
10.	Dendritic microstructure on sample 3A and at a weld pass.	13
11.	Dendritic microstructure at weld passes on sample 3B and high magnification micrographs at the respective locations.	14
12.	Dendritic microstructure on sample 3B and high magnification of a region.	14
13.	Dendritic microstructure observed on the surface of sample 3A at magnifications of 100×, 200×.	15
14.	Micrograph showing one of the matrix precipitates observed on the surface of sample 3A and EDX spectra resulting from the bulk and the precipitate.	15
15.	Micrographs showing the microstructure on plane 3A, matrix and grain boundary precipitates, and EDX spectra resulting from the bulk and grain boundary precipitates.	16
16.	Ti-rich precipitates in the weld and maps showing the topography at the locations where the high magnification micrographs were taken.	17
17.	Micrographs showing the heat-affected zone and high magnification micrographs showing precipitates in the heat-affected zone.	18
18.	OIM map of the weld on plane “B”, sample 3B; the same OIM map showing the orientation of each grain; and legends for crystal directions and the resulting grain boundary character distribution.	19
19.	OIM map on the surface of sample 3B and the resulting grain boundary character distribution.	20

20.	The same OIM map as in Fig. 19 showing crystal directions and SEM micrograph illustrating the dendritic microstructure of the weld.....	21
21.	Schematic showing the two planes on which the OIM characterization was carried out: plane “A”, along the direction of the dendrites, and plane “B”, perpendicular to the direction of dendrites.	21
22.	OIM maps from plane “A”, parallel to the direction of dendrites, and resulting grain boundary character distributions.	22
23.	OIM maps from plane “A” showing the grain orientations, and legends for grain orientations and grain boundary character distributions.....	23
24.	OIM map from plane “B”, perpendicular to the direction of dendrites, map showing the grain orientations, and legends for grain orientations and grain boundary character distributions.	24
25.	Grain boundary character distribution for laboratory-prepared welds.	25
26.	OIM map from Alloy 600, map showing the grain orientations, and legends for grain orientations and grain boundary character distributions.....	26
27.	Crack length vs. time for Alloy 182 SMA weld–metal specimen CT31-W01 TS in simulated PWR environment at 320°C during test periods 1–4a, 4b–5, 6–8, 9, and 10.	28
28.	Photomicrograph of the fracture surface of specimen CT31-W01 TS.	29
29.	A higher magnification photomicrograph showing entire crack extension in a region in the center of the specimen CT31–W01 TS. Micrographs b, c, and d are from locations 3, 2, and 1 in micrograph.	30
30.	Transition from TG to IG fracture and higher magnification micrograph of the boxed area showing the tip of a few cracks.	31
31.	Mixed TG and IG fracture modes, high magnification micrograph of the boxed area, and micrographs showing the crack tips at locations “1” and “2” in micrograph.	32
32.	Photomicrographs detailing the fracture in a region during test periods with a hold time and/or a high rise time and high magnification micrographs of positions indicated by arrows.....	33
33.	Photomicrographs detailing the fracture in a region during test periods with a hold time and/or a high rise time, and high magnification micrographs.....	34
34.	Crack length vs. time for Alloy 182 SMA double–J weld specimen CT31-W02 TS in simulated PWR environment at 320°C during test periods 1–3 and 4–5.	35
35.	Fracture surface of specimen CT31-W02 TS.....	36
36.	Micrographs showing the cross section of CT31-W02 TS.	37

37.	Crack length vs. time for laboratory-prepared Alloy 182 weld specimen CT933-TS in simulated PWR water at 320°C during periods precracking-period 2, 3-4, 5-6, 7-8, and 9-10.....	38
38.	Crack front in cross section of sample CT933-TS.....	40
39.	Crack front on fracture surface of sample CT933-TS.....	40
40.	Crack front on sample CT933-TS, where several fracture modes are identified: transition from TG to IG; IG; and ductile rupture in the IG region.....	41
41.	Crack length vs. time for Alloy 182 weld specimen CT933-TL in simulated PWR environment at 320°C during test periods precracking-1, 2, 3-4, 5, 6-10, 11, 12-14, 15, 16-19, and 20-21.....	43
42.	Fracture surface of Alloy 182 weld specimen CT933-TL. The regions dominated by IG fracture corresponding to the constant load periods are indicated in the figure.....	47
43.	Intergranular fracture on the Alloy 182 weld specimen CT933-TL resulting from the constant-load period CL-5.....	47
44.	Higher magnification image of IG fracture on the Alloy 182 weld specimen CT933-TL resulting from the constant load period CL-5.....	48
45.	Crack length vs. time for Alloy 182 weld specimen CT933-LS in simulated PWR environment at 320°C during precracking and periods 1-2, constant load period 3, and constant-load period 4.....	49
46.	Crack front on fracture surface of sample CT933-LS.....	50
47.	Transition from TG to IG observed on the fracture surface of sample CT933-LS.....	51
48.	Cross section and SCC area of CT31-W02 TS.....	52
49.	SEM image of the cross section of CT31-W02 tilted by 70° for OIM analysis.....	53
50.	SCC region of specimen CT31-W02 and resulting OIM map.....	53
51.	Cross sections of the three samples from CT933-TS tilted by 70° for the OIM analysis: CT933-TS-S1, CT933-TS-S2, and CT933-TS-S3.....	54
52.	SCC regions and resulting OIM map for CT933-TS-S1, CT933-TS-S2, and CT933-TS-S3..	54
53.	Fractions of cracked boundaries as a function of boundary type.....	56
54.	Fractions of cracked boundaries as a function of the relative orientation of the adjacent grains.....	57
55.	Experimental values of fatigue crack growth rate of Alloys 182 and 52 in air as a function of those estimated for Alloy 600 under the same loading conditions.....	59
56.	Fatigue CGR data for Alloy 82 and Alloy 182 weld metal in PWR environment as a function of the growth rate for Alloy 600 in air under the same loading conditions.....	60

57.	Fatigue CGR data for Ni–alloy welds in PWR environment as a function of the growth rate for Alloy 600 in air under the same loading conditions.	60
58.	CGR data for Alloy 182 SMA weld–metal specimen in simulated PWR environment at 320°C as a function of growth rates for Alloy 600 in air.	61
59.	Comparison of the SCC crack growth rate for the Argonne Alloy 182 weld with the available data for Alloy 182 and 82 welds in simulated PWR environment.	62
60.	Experimental crack growth rates in Alloy 182 weld in TL and TS orientations.	64
61.	Influence of the orientation of the dendrites on the crack growth rates in Alloy 182 and 82 welds in PWR environments.	64
62.	SCC crack growth data for the Argonne Alloy 182 weld specimens tested.	64
63.	Experimental crack growth rates of Alloy 182 and 82 welds obtained with and without periodic partial unloading.	67
64.	Temperature dependence of the CGR data for Alloy 182 and 82 obtained at Westinghouse, Lockheed Martin, Bechtel Bettis, ETH, and CEA at temperatures between 290 and 360°C. .	69
65.	Experimental crack growth rate normalized to 325°C as a function of stress intensity factor K	70
66.	Estimated cumulative distribution of the normalized parameter α in the CGR relationship for Alloy 182 based on data that satisfy the screening criterion of Ref. 52 and all the data. ...	71
67.	Distributions of the 95th, 90th, 67th, and 50th percentile values for parameter α for heats of Alloy 182 welds in PWR water at 325°C.	74
68.	Comparison of the SCC crack growth rate for Alloy 182 and Alloy 82 welds in simulated PWR environment with the 75th percentile curve.	74

Tables

1.	Chemical composition of Alloy 600 base metal and Inconel 182 and 82 weld metals.	3
2.	Welding process and conditions for various weld passes.....	4
3.	Chemical compositions of the bulk and matrix precipitate resulting from EDX analysis.	16
4.	Chemical compositions of the bulk and grain boundary precipitate resulting from EDX analysis.....	17
5.	Crack growth data for specimen CT31-W01 TS of Alloy 182 SMA weld in PWR water at 320°C.	27
6.	Crack growth data for specimen CT31-W02 TS of Alloy 182 SMA weld in PWR water at 320°C.	35
7.	Crack growth data for specimen CT933-TS of Alloy 182 SMA weld in PWR water at 320°C.	38
8.	Crack growth data for specimen CT933-TL of Alloy 182 SMA weld in PWR water at 320°C.	42
9.	Crack growth data for specimen CT933-LS of Alloy 82 SMA weld in PWR water at 320°C.	49
10.	Cracking data for both CT933-01 and CT31-W02.....	55
11.	Fractional errors in the population of cracking susceptible HABs as a function of alloy, orientation, and crack advance.	66
12.	Values of the parameter A in the Scott model for crack growth rate for several Alloy 182, 82, and 132 welds.....	72
13.	Values of the parameter α for Alloy 182 and 82 at 325°C as a function of the percentage of the population bounded and the confidence level.	73

Intentionally Left Blank

Executive Summary

The Ni–base alloys used as construction material in light water reactors (LWRs) have experienced stress corrosion cracking (SCC). Such cracking was first observed in steam generator tubes, but it has also occurred in Ni alloys used in applications such as instrument nozzles and heater thermal sleeves in the pressurizer and penetrations for control–rod drive mechanisms (CRDMs) in the reactor–vessel closure heads. In operating plants, the weld metal Alloys 82 and 182 are used with Alloy 600 and appear to be more resistant to environmentally assisted cracking than the wrought alloy. However, laboratory tests indicate that in pressurized water (PWR) coolant environments, the SCC susceptibility of Alloy 182 may be greater than Alloy 600, and Alloy 82 may be comparable to Alloy 600. This apparent inconsistency between field and laboratory experience has been an issue that needs further investigation.

A program is being conducted at Argonne National Laboratory (ANL) to evaluate the resistance of Ni alloys and their welds to environmentally assisted cracking in simulated LWR coolant environments. This report presents crack growth rate (CGR) results for Alloy 182 weld metal alloys in simulated PWR environments at 320°C. The tests were performed using specimens from both double “J” joint and deep-groove filled laboratory-prepared welds. The total crack extensions estimated by the DC potential method were verified by physical measurements on the fracture surfaces.

Metallographic examinations were performed to characterize the microstructure of the weld. The weld structure consists of vertically aligned columnar grains and dendrites. The weld microstructure was also examined by orientation imaging microscopy (OIM), a diffraction-based technique, to determine the orientations of the grains and the type of grain boundaries present. The results show that a large proportion (70%) of the grains boundaries are random or high-angle boundaries (HABs), which are more susceptible to cracking than those in specific orientation relationships, also known as coincident site lattice (CSL) boundaries. In addition, the OIM maps show the presence of clusters of grains that share similar orientations.

The environmental enhancement of CGRs under cyclic loading was determined relative to the CGRs that would be expected under the same loading conditions for Alloy 600 in air. In general, the CGRs of Alloy 182 in the PWR environment are a factor of ≈ 5 higher than those of Alloy 600 in air under the same loading conditions. This result is independent of rise time or frequency in the test conditions and indicates little or no environmental enhancement of CGRs of the Alloy 182 weld metal in the PWR environment under this type of loading condition. The experimental CGR for the laboratory–prepared Alloy 182 weld under trapezoidal loading (i.e., essentially a constant load with periodic unload/reload) is close to the mean value of CGR for Alloy 600 for the corresponding value of stress intensity factor (K) in a PWR environment. Most of the existing CGR data for Alloy 182 and 82 welds are a factor of 1–10 greater than the median value for Alloy 600.

Crack growth tests were conducted on 1–T compact tension specimens in TS, LS, and TL orientations, i.e., crack plane along or perpendicular on the columnar grains. The results show that the effect of sample orientation on the crack growth rate can be as high as a factor of four.

Metallographic examination of the fracture surface revealed relatively straight crack fronts. The fracture modes correlated well with the test conditions. High rise times or long hold periods favor intergranular (IG) SCC. Also, IG cracking apparently advanced more readily along some grain orientations than others, resulting in crack fronts with occasional unbroken ligaments and few regions of transgranular (TG) cracking.

The effects of grain boundary type and grain orientation on the cracking behavior of Alloy 182 weldments were examined. It was hypothesized that a boundary with a weak Taylor-factor mismatch, as would be the case for two neighboring grains that share a similar orientation, would be less susceptible to deformation and, ultimately, to cracking. By contrast, a strong mismatch in the Taylor factor across a grain boundary would tend to result in a strain incompatibility at that boundary, making it susceptible to cracking. To test the hypothesis, OIM maps were obtained along the crack paths in two compact tension specimens of Alloy 182. Comparison of scanning electron microscopy photomicrographs of the cracks with the OIM maps of the same areas enabled the identification of the types of cracked grain boundaries, as well as the relative orientation of the neighboring grains. The results showed that, on average, 90% of the cracked boundaries are HAB, and 87% of the cracks occurred along grain boundaries that separated dissimilarly oriented grains.

The existing CGR data for Ni–alloy weld metals (i.e., Alloys 82, 182, 52, 152, and 132) have been compiled and evaluated to establish the effects of material, loading, and environmental parameters on CGRs in PWR environments. The results from the present tests were compared with the existing CGR data.

The data in the literature, while limited, and the results from the present study indicate very little dependence of the environmental enhancement of CGRs on frequency and strain rate under cyclic loading in PWR environments for Alloy 182 and 82 welds. Under similar loading and environmental conditions, strain–rate–dependent environmental enhancement is observed in CGRs for Alloy 600.

In general, the CGRs of Alloy 182 are higher than those of Alloy 82. Although the results have substantial scatter, it is clear that weld orientation has a strong effect on CGRs. Crack growth rates along the plane of the columnar grains are higher in directions parallel to the columnar grains than in directions perpendicular to the columnar grains. The activation energy for the temperature dependence of SCC CGRs for Alloy 182 and 82 weld metals may be slightly higher than that for Alloy 600. Individual data sets yield activation energies of 120–250 kJ/mol (28.5–59.5 kcal/mol). Studies on the effect of dissolved hydrogen content indicate that CGRs in Alloy 182 and 82 welds are highest at dissolved hydrogen contents that result in electrochemical potentials close to the Ni/NiO phase transition.

The dependence of SCC growth rates of Ni–alloy welds on the stress intensity factor K can be represented by the Scott model. Material heat–to–heat variations of the CGR are considered and represented in terms of variability in the parameter A in the Scott model. The available data was used to estimate the cumulative distribution of A for the population of Alloy 182 and 82 welds. Values of the parameter A as a function of the percentage of the population bounded and the confidence level are presented. The results suggest that under similar loading and environmental conditions, the mean CGRs for Ni–alloy welds appear to be a factor of ≈ 2 higher than the mean CGRs for Alloy 600.

Acknowledgments

The authors thank E. J. Listwan J. Tezak, R. Clark, and T. M. Galvin, for their contributions to the experimental effort. This work is sponsored by the Office of Nuclear Regulatory Research, U.S. Nuclear Regulatory Commission, under Job Code Y6388; Program Manager: W. H. Cullen, Jr.

Intentionally Left Blank

Abbreviations

ANL	Argonne National Laboratory
ASME	American Society of Mechanical Engineers
ASTM	American Society for Testing and Materials
BWR	Boiling Water Reactor
C	Circumferential
CF	Corrosion Fatigue
CGR	Crack Growth Rate
CRDM	Control Rod Drive Mechanism
CSLB	Coincident Site Lattice Boundary
CT	Compact Tension
DO	Dissolved Oxygen
ECP	Electrochemical Potential
EDX	Energy Dispersive X-ray
GBC	Grain Boundary Coverage
GBCD	Grain Boundary Character Distribution
HAB	High Angle Boundary
IG	Intergranular
L	Longitudinal
LWR	Light Water Reactor
MRP	Materials Reliability Performance
NRC	Nuclear Regulatory Commission
NWC	Normal Water Chemistry
OIM	Orientation Imaging Microscopy
PWSCC	Primary Water Stress Corrosion Cracking
PWR	Pressurized Water Reactor
R	Radial
RCS	Reactor Coolant System
RPV	Reactor Pressure Vessel
RTZ	Rolled Transition Zone
SA	Solution Annealed
SCC	Stress Corrosion Cracking
SEM	Scanning Electron Microscopy
SHE	Standard Hydrogen Electrode
SS	Stainless Steel
TG	Transgranular

Intentionally Left Blank